

# INVESTIGATING ACTIVE VORTEX GENERATORS AS A NOVEL HIGH LIFT DEVICE

Tomas Melin\*, Simone Crippa\*, Martin Holl†, Miroslav Smid†

\*Department of Aeronautical and Vehicle Engineering, Royal Institute of Technology, KTH.

†VZLU - Vyzkumny a zkusebni letecky ustav, a.s. Aeronautical Research and Test Institute.

**Keywords:** *Vortex Generators, High-Lift, Flow Control.*

## Abstract

Within the framework of the HELIX programme [1], a study using experimental and numerical tools was employed to simulate the aerodynamic behavior of a transport aircraft wing profile when equipped with deployable Active Vortex Generators (AVGs). The geometry of the investigated concept consists of a single row array of delta wings positioned above the main airfoil, close to the leading edge, see figure 1. The operational hypothesis of this concept is that the vortex pair generated by the shear layer roll-up at the leading edge of the delta wing will translate downwards. Previous wind tunnel results, obtained for a different wing profile, were promising [5], indicating a possible gain in maximum lift coefficient  $C_{Lmax}$  of about 0.3 with only small increment in drag and beneficiary stall characteristics.

The numerical simulations performed were divided into three different cases: cruise, takeoff and landing configurations. The numerical simulation set-up was a 2.5 dimensional workspace, extruding the profile to a width of one vortex generator.

An experimental validation was performed at VZLU:s three meter open low speed tunnel facility. The wind tunnel measurements were performed at a Reynold's number of  $1.65 \cdot 10^6$ .

The results of the investigation showed that the

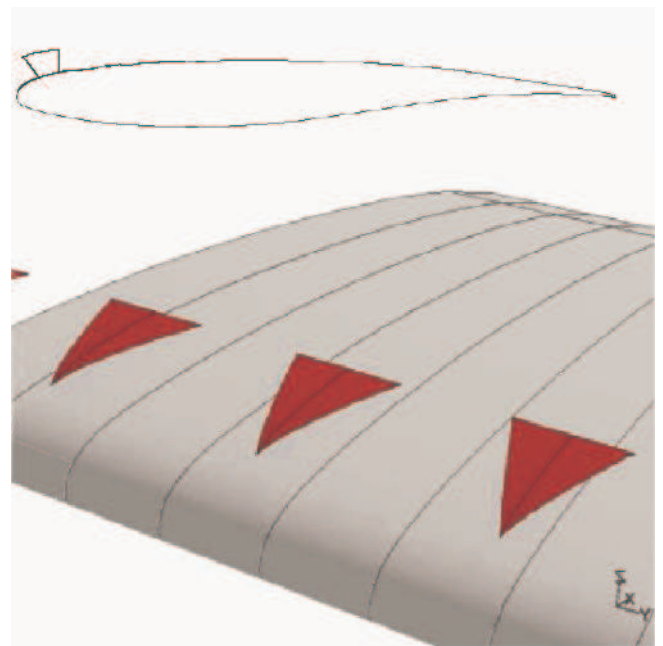


**Fig. 1** Investigated late generation wing profile and the active vortex generator array. AVG chord are 10% of the root chord of 4159 mm. The airfoil is an A320 derivative profile.

baseline profile, without the AVGs mounted, produced a higher  $C_{Lmax}$  and a lower drag than the concept investigated. Possibly, the stall behavior of the AVG concept could be said to have better characteristics than the baseline. The conclusion is that the AVG cannot replace the slat on a late generation wing profile.

## 1 Introduction

This report describes the investigation of the use of active vortex generators (AVGs) on a high speed commercial transport as described in the *Helix* baseline document [2]. The work is primarily focused on a numerical study of the flow field around a wing section equipped with delta shaped AVGs. An experimental test was set up to provide additional validation data. Some of the numerical work herein has previously been reported in [10] and [11].

Vortex generation systems are prevalent methods for boundary layer control both in channel flow, such as intake ducts [12], and flap gaps. These methods are already in use on several contemporary aircrafts. Usually the vortex generators are small devices of varying shape and geometry, protruding from a wing or other surface where the aerodynamic behavior is important, ([7] [8]) as cited in [6]. These devices induce vortical motion in the fluid around the surface. The vortex is usually embedded in the boundary layer, providing a mixing mechanism that is capable of reenergizing the flow at the near wall region. The vortex mixes the boundary layer with high energy free stream air, as well as adding momentum to the boundary layer through the vortex core. The induced energy stabilizes the boundary layer, keeps the flow attached and delays separation to higher angles of attack. However, vortex generating devices can be much larger. Some examples are the DC-10 nacelle strakes or the F-18 Hornet leading edge strakes (although, in the latter case the purpose of the device is also lift generation). There are several add-on or retrofitting kits available for general aviation aircraft. Usually these devices are intended to increase low speed performance of the aircraft [13].

The design reviewed in this study is a vortex generator which consists of a single row array of small delta wings positioned above the main airfoil, close to the leading edge and well above the boundary layer, see figure 2. The AVGs are re-

tractable by a servo mechanism and stows in the main wing, just ahead of the forward wing spar. This allows for a minimization of cruise drag, as the AVGs would not be exposed to the free stream air during cruise. By changing the angle of attack of the AVG, the deployment mechanism also provides a way of regulating the vorticity production, and hence the amount of boundary layer control.



**Fig. 2** Picture of the experimental setup at VZLU, showing the vortex generator array at the leading edge of the wing profile.

The size of the AVG is in the order of 10% of the local chord, see figure 3. The underlying configuration is based on a US patent [3] and subsequent articles [4] and [5], but the primary function is quite different. The investigated vortex genera-

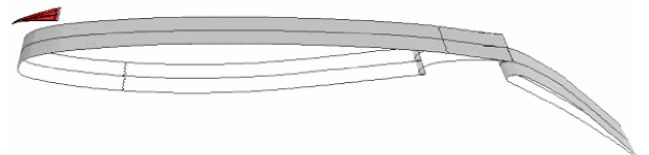


**Fig. 3** Single vortex generating delta positioned above main airfoil. The trailing edge flap is in the landing configuration.

tor has, in order to conform to the wing upper surface skin, a camber that allows it to have zero local angle of attack along its span in the curved air stream near the leading edge. The same servo

mechanism that provides the deployment is also used to change the angle of attack of the AVG to accommodate a variable vorticity production.

## 2 Numerical Study

In the two cases below, the methodology is described for both the HELIX baseline and the AVG study. However, due to the large numerical similarities between the different cases, only one cruise case and one landing cases are discussed in detail. However, comparative results for all simulations are presented in the result section.

### 2.1 Meshing

The mesh generator used for all the models was the commercially available code *ICEM CFD*. Using the various modules of this widely known engineering tool, all the geometries could be meshed. For the less complicated geometries of this study, a structured meshing approach was possible. *ICEM CFD HEXA*, a semi-automated meshing module, was employed. This allowed a rapid generation of multi-block structured and unstructured hexahedral volume meshes. The underlying block topology model was generated directly on a given CAD geometry.

After interactively creating a 3D block topology model equivalent to the geometry, this block topology may be further refined through splitting of edges, faces and blocks. Additionally, there are tools for moving the block vertices, individually or in groups, onto associated curves or CAD surfaces. The user may also associate specific block edges with CAD curves to capture important geometric features in the mesh.

*HEXA* provides a projection based mesh generation environment where, by default, all block faces between different materials are projected to the closest CAD surfaces. Block faces within the same material may also be associated to specific CAD surfaces to allow the definition of internal walls. The required cell distributions are obtained through edge meshing tools.

For the more complicated geometries, in this case the traditional high lift configuration with a slat an flap and the AVG concept, another meshing approach was necessary. The prohibitively high cell number of a completely unstructured mesh led to a hybrid mesh approach, consisting of a structured mesh for the far field discretization and an unstructured mesh for the near field discretization. The far field hexahedral mesh was also generated with *HEXA*, but for the near field another module, *TETRA*, was used to generate tetrahedral volume cells. An overview of the computed cases can be seen in 4.

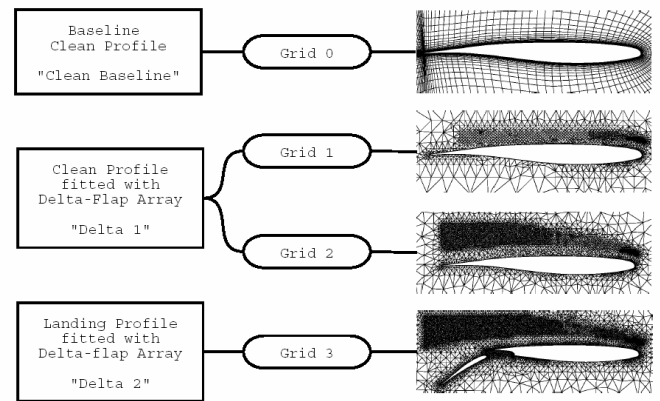


**Fig. 4** Mesh type overview, not shown are the baseline takeoff and baseline landing, or the concept take off configuration. (Symmetry plane for grids 1-3).

## 3 Helix Baseline

As described in the introduction, the first step of the main part of the project was recognized to be a computational analysis of the aerodynamic performance of the HELIX baseline profile. This calculation was needed to generate the data that was to be compared with the later step of the project, the investigation of the effect of the AVG array. This was done considering geometric and Reynold's number similarity. The wing section at the kink of the wing trailing edge was identified as a characteristic section, since further examination had to deal with an unswept, infinite wing. To gain the aerodynamic performance of

this profile, a 2D calculation would be sufficient. However, in order to use the same solver settings as in the later simulations, the geometrically simple model presenting only curves was extruded to a 3D volume with an increase in complexity due to the required bounding surfaces. The relatively low complexity of the geometry led to a C-H structured mesh.

### 3.1 Geometry and Assumptions

The clean baseline wing control surfaces are not well defined exactly at the kink, so the wing section to be analyzed was chosen slightly more out-board than the kink. The taper reduces the profile chord length to 4,128 mm rather than 4,159 mm given in the baseline document [2]. Figure 5 shows the *HELIX* baseline aircraft configuration with the chosen section.

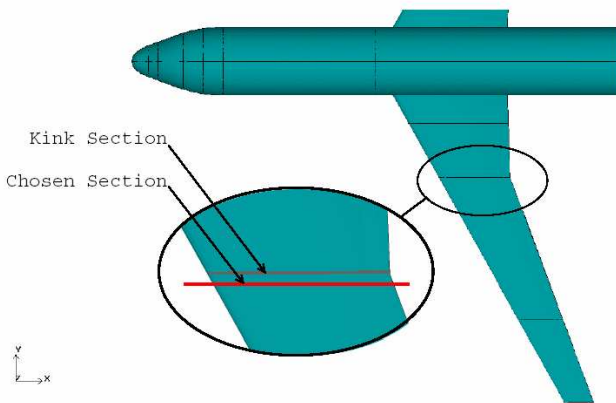


**Fig. 5** Baseline aircraft geometry, top side. The wing section used for the 2D analysis is marked.

The span of the unswept wing in the 2.5D setup was chosen to be equal to the chord. The domain boundaries were set at ten times the chord both upstream and downstream of the profile. The domain inlet far field surface was chosen as a parabolic to avoid discontinuities in the input surface.

### 3.2 Solver Settings

The commercial solvers *Fluent* and *EDGE V3.1* were used in the simulation. The segregated solver was used for the calculations, as the eval-

uation of the coupled solvers revealed convergence problems. The realizable k-epsilon turbulence model was used with a standard wall function near-wall treatment since it allowed secure and fast calculations. The ideal-gas law was used as density model and the Fluent standard Sutherland's law was used as viscosity equation. Although the temperature gradients were expected to be fairly low, Sutherland's law yields better results. A gauge pressure of 1,013.25 hPa was set near to the inflow boundary.

### 3.3 Computation

In order to achieve a better solution convergence, it proved to be more favorable to run the first 50 iterations resolving only the flow and energy equations without the turbulence equations. The turbulence modeling was then switched on for the remaining iterations until convergence was achieved between approximately 2000 to 3000 iterations. Convergence was defined as no change in force coefficients up to the 2nd digit for 100 iterations, and no change in the residuals attitude. Residuals convergence was always achieved before force coefficients convergence.

The computations using the segregated solver were run on single processor on Roxette, a cluster of 16 dual Pentium III nodes at the center for parallel computers ([www.pdc.kth.se](http://www.pdc.kth.se)) at KTH. The low cell number of this grid resulted in a high calculation speed of approximately seven seconds per iteration. This low count justified not doing a parallelization effort.

## 4 Active Vortex Generator Array

### 4.1 Problem Description and Approach

The AVG system was to be fitted on the *HELIX* baseline configuration. For the reasons given above, and for comparison with the calculated data, the kink profile was also used in this case. The performance of the AVG system depends on the location, strength and downstream development of the generated vortices. This, on the other hand, depends on the geometric parameters

of the vortex generators, such as the chord wise position, the distance from the surface, the leading edge length, angle of attack and shape.

In order to prove the feasibility of the system, a first configuration had to be determined. The shape of the vortex generators was chosen to be a delta plan-form for simplicity reasons. The requirement of being able to withdraw the vortex generators into the wing surface leads to a cambered delta flap surface.

A simple deployment mechanism without any leverage could not deploy the AVG into the flow field more than the local wing thickness. Since the flow field around the baseline configuration was known from the previous calculations, it was possible to see that the highest expected local angle of attack of the AVG would be achieved by deploying it as far away from the wing surface as possible.

The structure of the flow over a AVG wing mainly depends on three parameters that are coupled with each other. The angle of attack, the free stream Mach number and the AVG leading edge sweep angle. With a fixed angle of attack and Mach number, the only parameter that can be varied to influence the flow structure is the sweep angle. A low sweep angle leads to the formation of a separation bubble at the leading edges of the AVG, a structure which must be avoided in this study, as this would prevent the formation of the leading edge vortices. Increasing the sweep angle leads to the rolling up of the shear layer on the wings top side, resulting in the formation of the required vortices, see figure 6.

## 4.2 Geometry

The maximum AVG chord length was determined by the AVG leading edge side, by an optical estimation of the highest acceptable curvature and on the trailing edge side by an estimation of the position of the forward wing spar. To obtain preliminary fail-safe results, the AVG chord was chosen to be as long as

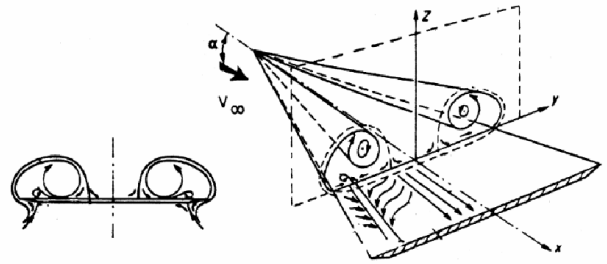


Fig. 6 Rolled up vortices on a delta wing, from [9].

possible to develop the highest possible vortex strength. Projected on the x-y-plane, the AVG chord length became  $c_f = 332.96mm$ .

Fixing the chord length to the maximum possible value also defines the chord-wise position of the AVG apex. Having a relatively low free stream Mach number of 0.2 and an expected low relative angle of attack of the AVG, results in the requirement of using a relatively high sweep angle. For possible future comparison with other studies, a sweep angle of  $70^\circ$  was chosen. The AVG span projected on the x-y-plane was computed to  $s = 242.38mm$ .

The thickness of the AVG was arbitrarily set to seven millimeters, since the thickness is known not to be very important for the vortex development over a laege range, .

The bevel angle of  $15^\circ$  was chosen for possible future comparison reasons, since it is the most commonly used value. The height of the AVG leading edge apex above the wing surface was set to 206 mm, translating it normal to the wing surface. This results in positioning the AVGs as far upstream as possible, a position where the relative angle of attack should be at its highest and where as little wing surface as possible is shaded by the AVG.

A wide space between two neighboring AVG was recognized to be preferable by [4]. But a large distance is also probable to have negative effects on the performance enhancement of the vortex

generators array. The span-wise AVG density was set to a value of 0.5. This was achieved by extruding the slatless wing profile to a width of 242 mm and applying a symmetry boundary condition here and at the AVG centerline.

The vortex generators array fitted on the baseline profile of the calculations can be seen in figure 7.



**Fig. 7** Profile Geometry, AVG wing landing configuration.

### 4.3 Mesh

The first mesh for this configuration, grid 1, has a total of 379,998 cells. This hybrid mesh is divided into 7,120 hexahedral, structured cells in the far field, and in 372,878 tetrahedral, pyramid and prism unstructured cells in the near field region. Figure 8 shows the near field mesh, and figure 9 shows the different zones of refinement.

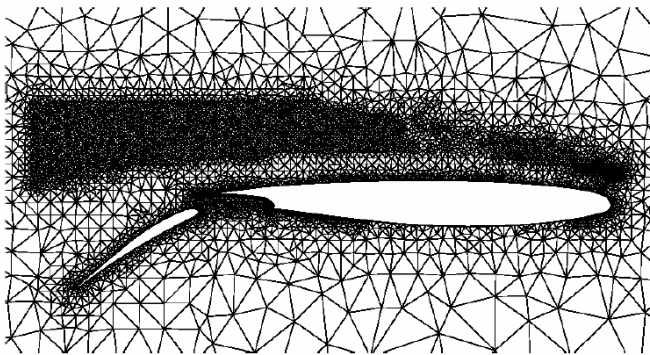


**Fig. 8** Near field mesh.

### 4.4 Computation

For the computations with the second mesh, convergence was achieved smoothly and with a maximum of 4,000 iterations for the higher angles of attack. Since the flow field was developed fairly

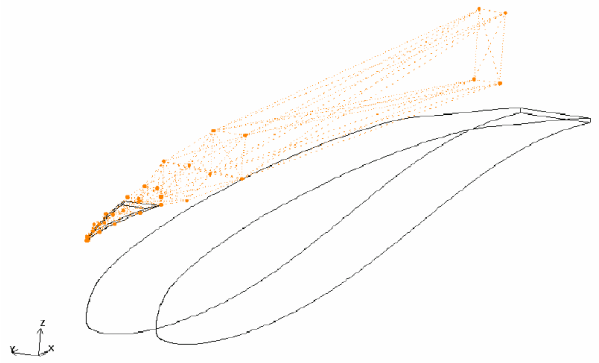


**Fig. 9** Refined mesh region behind the AVG.

slowly, these calculations were considered converged when the change of lift coefficient was less than 0.001 for the last 100 iterations. The computations ran on multiprocessor on two to four Roxette nodes, depending on the availability of Fluent licenses. The computation time changed from 18 seconds per iteration to 8 seconds per iteration for the second grid.

### 4.5 Parametric Study

The sensitivity of the system was investigated with a parametric study, simulating different separation distances between AVG and the main airfoil as well as the geometric angle of attack of the AVG. Figure 10 shows the different computed cases. Three different heights: 208, 182 and 165 millimeters and at four different incidence angles  $-12.88^\circ$ ,  $-9.88^\circ$ ,  $-6.88^\circ$  and  $-3.88^\circ$  respectively. The  $-12.88^\circ$  case was a parallel translation of the AVG from the main wing upper surface, while the other was a translation plus rotation.

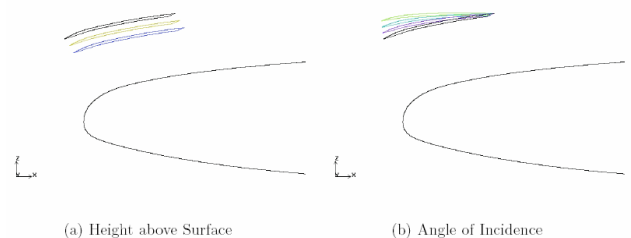


**Fig. 10** Parametric study cases.

## 5 Experimental method

The influence of active vortex generators was measured on a quadrangular model of a wing with circular end plates, the chord length 0.6 m. The tests were performed in the three meter diameter low speed wind tunnel at VZLU, Aeronautical Research and Test Institute in Prague (Czech Republic). The wind tunnel used was an atmospheric open section, closed return. All tests were performed at the Reynold's number  $1.65 \cdot 10^6$ . The aerodynamic coefficients measured, such as lift coefficient, drag coefficient and pitching moment coefficient, were calculated by standard methods with conventional definitions. The general layout can be seen in figure 11.



**Fig. 11** Experimental setup of the 2.5 dimensional validation tests of the active vortex generator array.

Lift and drag was measured over a range of angles of angles of attack from -10 to +25 degrees for 12 different configurations, flaps stowed, at  $16.7^\circ$  take off and at  $32.4^\circ$  landing. For each of these cases, the AVG incidence was set at  $-12.88^\circ$ ,  $-9.88^\circ$ ,  $-6.88^\circ$  and  $0^\circ$  degrees.

The AVG incidence was measured as the difference between the AVG root chord and the main wing chord, positive upwards, as shown in figure 12.

## 6 Results

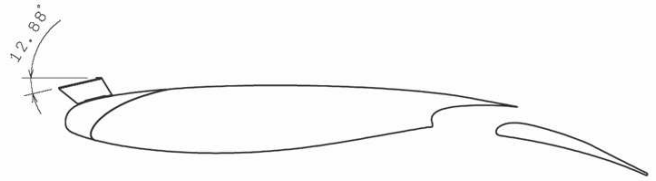


**Fig. 12** Definition of AVG incidence.

### 6.1 Baseline Results and Discussion

As the angle of attack was increased, the convergence of the calculations became more and more difficult. At an angle of attack of  $16^\circ$  force coefficient convergence was not achieved even after 13,000 iterations. The drag polar of the baseline cruise case is shown in figure 13.

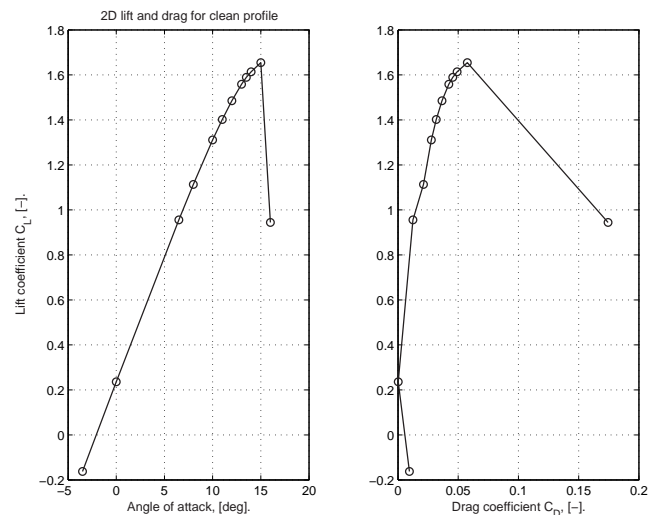


**Fig. 13** Clean baseline 2D drag polar.

The baseline profile showed an abrupt stall behavior at  $15^\circ$  angle of attack. Before the stall, a mainly attached flow field existed on the upper surface, as visible in the path line plot, see figure 14. A slight trailing edge separation is also visible. At  $16^\circ$  a dramatic change in the flow structure occurred. The trailing edge stall rapidly advances from to a fully developed stall. In figure 14 (b) the massive detached upper surface flow field is clearly visible. Complete drag polars were created for the baseline geometry in the cruise, takeoff and landing configuration.

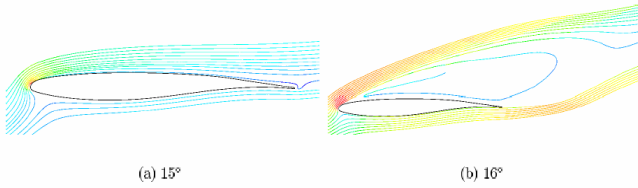


**Fig. 14** Baseline flow field at two different angles of attack.

**6.2 Active Vortex Generator Array Results**

Figure 15 shows the computational  $C_L$  vs. angle of attack for the active vortex generator concept in take off and in landing configurations. It can clearly be seen that the AVG concept provides a lower  $C_{Lmax}$  in the landing configuration and a slightly higher for the take off configuration. Upon studying the flow field more carefully, it can be appreciated that the stall behavior is characterized by a leading edge separation, probably due to the lack of a slat.

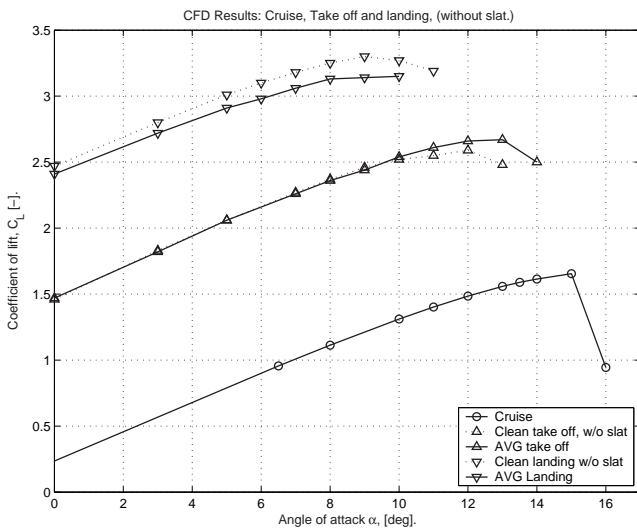


**Fig. 15** Lift coefficient vs. angle of attack for the AVG concept.

The parametric study was done with the flaps configured for landing. Figure 16 shows  $C_L/\alpha$  curves for different geometrical angles of attack of the active vortex generators.

Figure 16 shows that increasing the geometrical angle of attack of the vortex generator, and thus increasing the amount of generated vorticity

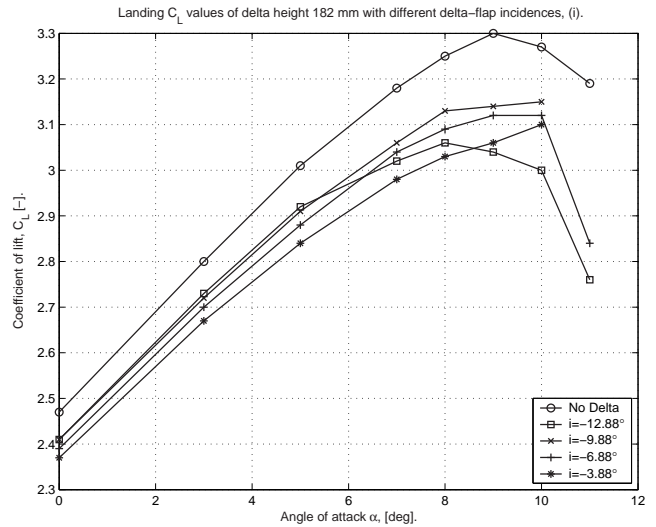


**Fig. 16**  $C_L$  vs. angle of attack for different geometric angles of attack of the AVG. Trailing edge flaps are in landing configuration.

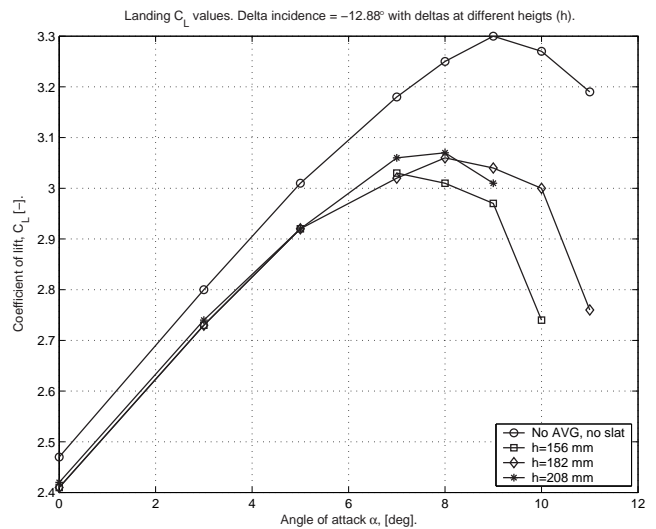


**Fig. 17** Influence of separation distances (h) on  $C_L$ .

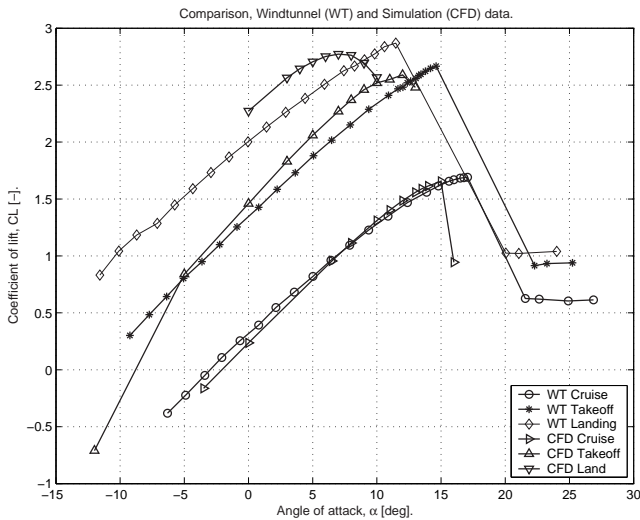
has a negative effect on the produced lift and maximum lift coefficient. Assuming that this is an absolute value effect, the best efficiency would be reached with the vortex generator producing no net vorticity (hence not being deployed).

Figure 17 shows the relation of the separation distance between the AVG and the main airfoil. It indicates that all separation distances give approximately the same negative offset in lift, with

no clear trend in stall behavior, which is in line with the leading edge stall.

### 6.3 Experimental Validation

The results of the numerical study and the experimental run with no AVGs attached compares as shown in figure 18 below. This figure contains data for cruise, takeoff and landing configurations.



**Fig. 18** Comparison between numerical and experimental results with the clean configuration, i.e. no Vortex generators attached

For the cruise configuration,  $C_{Lmax}$  is predicted well in value and behavior by the simulations. However, the CFD simulation under predicts the stall angle of attack by about two degrees.

For the takeoff configuration,  $C_{Lmax}$  is again under predicted by the simulation, this time by 0.1. The simulated stall seems smoother than the experimental. The CFD simulation under predicts the stall angle of attack by 2.5 degrees.

For the landing configuration,  $C_{Lmax}$  is again under predicted by 0.1 by the simulation and the simulated stall seems smoother than the experimental. The CFD simulation under predicts the stall angle of attack by 4.5 degrees.

In all cases, the lift slope of the simulated data

slightly is over predicted.

The case with the cruise flap setting i.e. stowed, is examined in figure 19. There is good agreement between wind tunnel (WT) and CFD in the linear part, but the  $C_{Lmax}$  is under predicted and the stall characteristic of the is smoother in the numerical simulation.

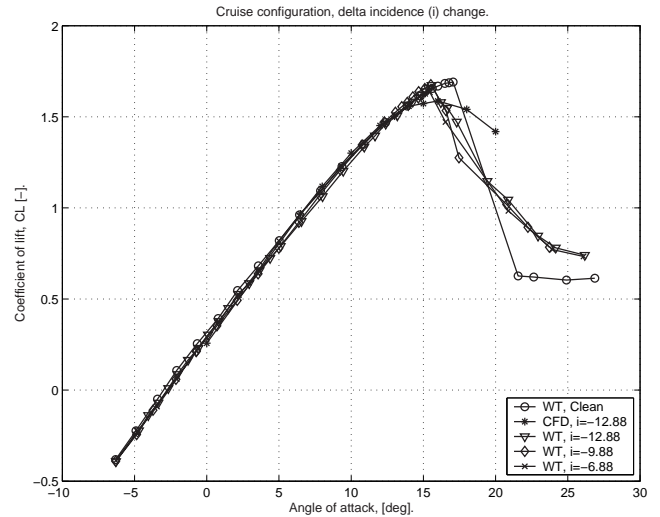


**Fig. 19** Cruise setting, comparison between wind tunnel experiments (WT) and computational results (CFD). Numbers indicate different settings of the vortex generators incidence in degrees.

The take off configuration results from wind tunnel and CFD are compared in figure 20. In this case, the computed CFD result is predicting the stall angle of attack properly, but over predicting  $C_{Lmax}$  with about 0.25.

Lastly, simulation and experiment results of the landing configuration is compared in figure 21, where again the  $C_{Lmax}$  is over predicted and the stall angle of attack is under predicted.

## 7 Conclusions

The efficiency of the AVG system depends on location and shape of the AVG. The height above the surface, the angle of incidence of the AVG and the AVG density are important parameters.

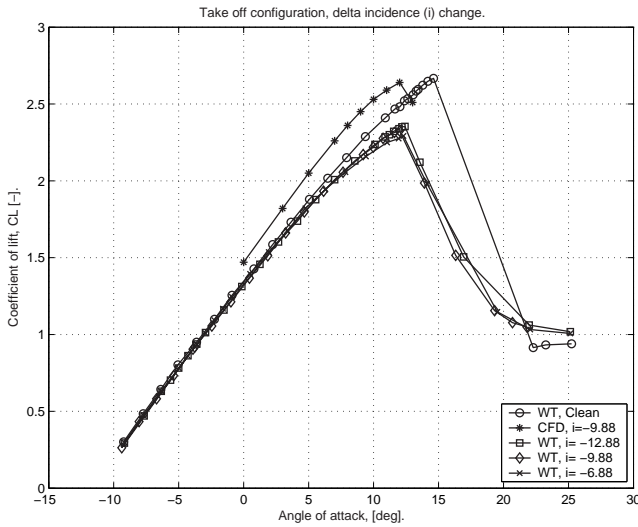


**Fig. 20** Take-off configuration, comparison between wind tunnel experiments (WT) and computational results (CFD). Legend numbers indicate different settings of the vortex generators incidence in degrees.

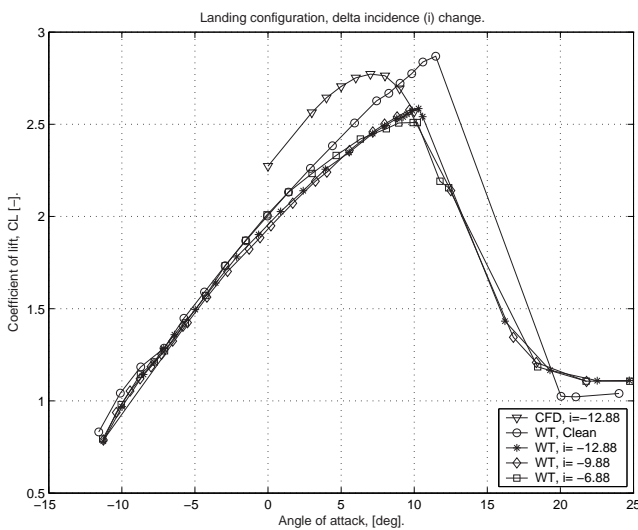


**Fig. 21** Landing configuration, comparison between wind tunnel experiments (WT) and computational results (CFD). Legend numbers indicate different settings of the vortex generators incidence in degrees.

The airfoil also plays a significant role. The camber of the profile, the flap deflections and the leading edge shape affect the velocity field around the AVG and have a large influence on its efficiency factor.

Out of this, two important optional parameters have been investigated in a CFD-analysis: the height of the AVG above the leading edge for a certain supercritical profile and the angle of incidence of the AVG. The airfoil investigated has the aerodynamic characteristics of an A320 profile.

In a coarse parametric study on the landing configuration three heights each with four different angles of incidence were computed. An improvement of the  $C_L$  values and of the stall behavior could not be determined due to artificial high velocities at the leading edge. Nevertheless the results lead to a better understanding of the AVG.

The mesh generator used in this study was *ICEM CFD*. The flow solver was *EDGE V3.1*. On the whole around twenty computational grids had been calculated in about 23,000h of computations occasionally on about 120 processors at the same time. The CPU time is portioned on Roxette, 12,109.8 hours, Strindberg, 8,279.9 hours, and Monolith, 3,019.5 hours.

The change of the flow solver from *Fluent6*, for which we had six licenses, to *EDGE* appeared as a necessary decision. This was verified by looking at the amount of calculated hours even though the introduction of the new flow solver required some set-up time. Normally a change of the flow solver should be avoided for later comparisons of the results.

The turbulence model *EARMS* [14] of Wallin and Johansson showed a good convergence and is recommended for further studies. The mesh is never perfect and many improvements can be done based on this study but the results were satisfying. All computed configurations showed remarkable high velocities at the leading edge, which were to some extent expected due to the missing leading edge device. A reduced camber of the profile with a less deflected trailing edge flap would reduce these velocities but result in a

negative loss of lift.

Pursuing studies may be carried out on different profiles with different leading edge radius. This could diminish the negative aspect on this profile. However, it has to be mentioned that the wing profile is optimized for cruise conditions. If the AVG array cannot be optimized for this configuration, the qualitative improvement of the AVG high-lift generation system for civil transport aircraft, which is purpose of this concept, has to be reconsidered.

In general, the missing leading edge devices lead to high velocities in the leading edge region. The ability of the AVG to rectify this behavior of the flow is questionable. Further studies of the effect of a camber of the AVG could be useful for a better understanding of the AVG system. The development of the vortex is a main point of the efficiency factor of the AVG system.

The validation runs in wind tunnel gave slightly different results than the numerical simulation in the take off and landing configurations. These discrepancies may be explained by the fastening method of the AVG:s in the experimental model. As no surface milling could be made, the AVG models were given a foot which was taped to the upper surface. This could disrupt the leading edge suction and produce an under prediction of the stall angle of attack in the experiment.

However, the agreement is good enough to allow decisions on both the experimental and the numerical data. Although they differ in absolute values, their qualitative description of the concept is the same. The aerodynamic performance of the helix baseline airfoil is degraded by the use of the proposed type of vortex generators.

## 8 Future Work

One idea of active vortex generators has been examined by Barret [15]. These so-called smart vortex generators (SVG) have a shape of reverse

AVG with a chord length of 1/10 of the airfoil chord length and the possibility to deploy at the leading edge. The benefit demonstrates an increase in  $C_{Lmax}$  of 14%, a rise of  $2.7^\circ$  in stall and low drag penalty. Further studies should concentrate on a combined system of vortex generation and leading edge device. The increase of weight, costs and complexity has to be included in these studies. These penalties have to be minimized while providing the required airplane takeoff and landing performance. Nevertheless, the adequate low speed performance will play an essential role in future aircraft designs and the effects are well investigated for twin engine transport.

## References

- [1] Helix Consortium, EU Contract, *GRD 12000-25205*, Annex 1, 2000
- [2] Simon Galpin, *HELIX/TM/AUK/SAG090701/4*, Airbus UK, 2001
- [3] Novak; Dieter K, *Aircraft wing flaps*, United States Patent: 5,772,155, May 15, 1997
- [4] Novak D.K. Solies U.P, *A High Lift Generation and Stall/Spin Recovery system*, NASA CR NAS1-98091, 1998
- [5] Novak D.K. Solies U.P, *Windtunnel Tests of a High Lift Generator and Stall/Spin Recovery System*, Journal of Aircraft, AIAA Vol 37, No 3, 2000.
- [6] Torbjörn Gustafsson, *Alternative approaches to rear end drag reduction*, TRITA-AVE 2006:13 ISSN 1651-7660, KTH, Stockholm, Sweden 2006
- [7] S. Klausmeyer, M. Papadakis, J. Lin, *A Flow Physics Study of Vortex Generators on a Multi-Element Airfoil*, AIAA 96-0548
- [8] W. Calarese, W.P. Crisler, G.L. Gustafson, *Afterbody Drag Reduction by Vortex Generators*, WPAFB, Ohio, AIAA-85-0354, Jan 1985, Reno, Nevada
- [9] Rom J, *High angle of attack aerodynamic*, Springer-Verlag, 1991.
- [10] Simone Crippa, *CFD Evaluation of a Novel Active Vortex Generation System*, Master Thesis, Skrift 2003-03, Dept. Aeronautical and Vehicle Engineering, Royal Institute of Technology (KTH), Sweden 2003.
- [11] Alexander Kolb, *CFD Analysis of a Novel Active Vortex Generation System*, Master Thesis, Skrift 2003-22, Dept. Aeronautical and Vehicle Engineering, Royal Institute of Technology (KTH), Sweden, 2003
- [12] Bruce J. Wendt, *Parametric Study of Vortices Shed from Airfoil Vortex Generators*, AIAA JOURNAL Vol. 42, No. 11, November 2004
- [13] Mike Busch, *Vortex Generators: Band-Aids or Magic?* <http://www.avweb.com/news/reviews/182564-1.html>, 2006-03-14 09:49 UTC
- [14] S. Wallin, A. Johansson, *An explicit algebraic Reynolds stress model for incompressible and compressible turbulent flows*, Fluid Mech. (2000), vol. 403, pp. 89-132
- [15] Barret R., Farokhi S., *Subsonic Aerodynamics*
- and Performance of a Smart Vortex Generator System*, Journal of Aircraft , Vol. 33, No. 2, March-April 1996, pp. 393-398.